Journal of Environmental Economics & Chemical Processes (JEECP)

https://doi.org/10.22034/jeecp.2026.2087835.1007

Journal Homepage: WWW.JEECPJournal.com

Journal of Environmental Economics & Chemical Processes (JEECP)

ORIGINAL RESEARCH PAPER

Comprehensive Review of Methanol-to-Olefins (MTO) Process: From Kinetic Modeling and CFD Simulation to Pilot-Plant Design and Construction

Mahdieh Garmsirian; Reza Mosayebi Behbahani *

Department of Gas Engineering, Ahvaz Faculty of Petroleum, Petroleum University of Technology (PUT), Ahvaz, Iran

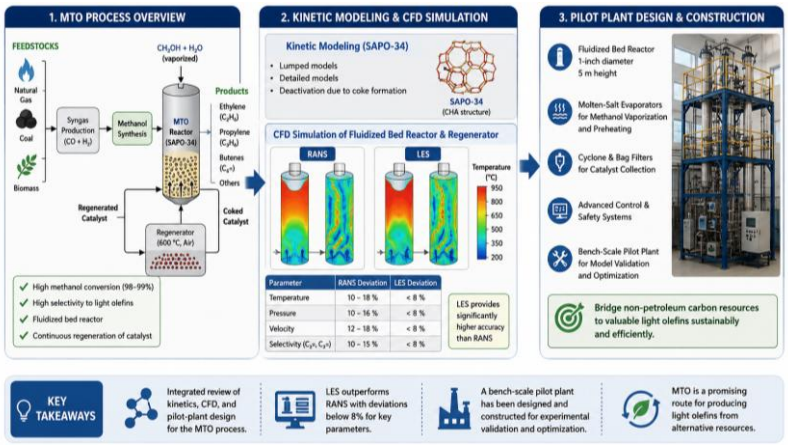
P A P E R I N F O

Paper history:
Received: 05/18/2026
Revised: 06/21/2026
Accepted in revised form: 06/30/2026
Published: 03/30/2027

***Keywords*:**
MTO;
SAPO-34;
Reaction Kinetics;
Fluidized Bed Reactor;
Catalyst Regenerator.

A B S T R A C T

The Methanol-to-Olefins (MTO) process serves as a key technology in the modern petrochemical industry, bridging non-petroleum carbon resources (natural gas, coal, biomass) with valuable light olefins (ethylene and propylene). This comprehensive review covers three main aspects of the MTO process: (1) kinetic modeling of the reaction over SAPO-34 catalyst, (2) Computational Fluid Dynamics (CFD) simulation of the fluidized bed reactor and catalyst regenerator with a comparison of LES and RANS approaches, and (3) design and construction of a bench-scale pilot plant. In the kinetics section, lumped and detailed kinetic models along with deactivation functions due to coke formation are reviewed. In the CFD section, simulation results show that the LES approach outperforms RANS significantly, with deviations below 8% for key parameters such as temperature, pressure, velocity, and selectivity, whereas RANS exhibits errors between 10–18%. In the design section, the technical specifications of an MTO pilot plant, including a 1-inch diameter, 5 m high fluidized bed reactor, molten-salt evaporators, catalyst collectors, and control systems, are described. This review serves as a comprehensive guide for researchers and engineers working on MTO technology.



1. Introduction

Light olefins (ethylene and propylene) are the primary building blocks of the polymer, petrochemical, and chemical industries. Traditional production routes, namely steam cracking of naphtha and fluid catalytic cracking (FCC), are heavily dependent on crude oil [1, 2]. Due to declining oil reserves, rising oil prices, and environmental concerns regarding CO_2 emissions, the petrochemical industry is shifting toward alternative feedstocks such as natural gas, coal, and biomass [3, 4].The Methanol-to-Olefins (MTO) process is a key technology in this transition. Methanol, which can be produced from syngas (CO, H_2), is converted over zeolite catalysts such as SAPO-34 into a mixture of light olefins [5]. SAPO-34, with its chabazite (CHA) structure and small pore openings, exhibits high selectivity to ethylene and propylene, although coke formation and gradual deactivation remain major challenges [6, 7]. Design and optimization of MTO reactors require a deep understanding of multi-scale phenomena: complex gas-solid two-phase flow, exothermic reactions, and catalyst deactivation. Computational Fluid Dynamics (CFD) has emerged as a powerful tool for simulating MTO reactors and regenerators [8, 9]. Two main turbulence modeling approaches exist: Reynolds-Averaged Navier-Stokes (RANS), which is computationally efficient but smooths out transient flow details, and Large Eddy Simulation (LES), which resolves large turbulent structures with higher accuracy but at significantly higher computational cost [10, 11]. In addition to modeling, the construction of bench-scale pilot plants

* Corresponding Author: Reza Mosayebi Behbahani
E-mail address: behbahani@put.ac.ir
ISSN:3116-0050
URL: https://www.jeecpjournal.com/article_736320.html

Please cite this article as: M. Garmsirian, & R. Mosayebi Behbahani, *Journal of Enviromental Economics & Chemical Processes (JEECP)*, 2027, *4*(1), 15-21. https://doi.org/10.22034/jeecp.2026.2087835.1007

/© 2027 The Author(s). Published by Power of New Vision Movement Institute.

is essential for model validation and determination of optimal operating conditions. In Iran, given vast natural gas reserves, development of MTO technical know-how is a national priority [12]. This review integrates knowledge from two major sources: a CFD progress report comparing LES and RANS for the MTO reactor and regenerator, and the final report on the design and construction of a bench-scale MTO pilot plant.

This review was conducted following a systematic literature search strategy. We searched the Web of Science, Scopus, and Google Scholar databases using the keywords: 'methanol-to-olefins', 'SAPO-34', 'kinetic modeling', 'CFD simulation', 'LES', 'RANS', 'fluidized bed reactor', 'catalyst regeneration', and 'pilot plant design'. The search covered publications from 1990 to 2025. Only peer-reviewed journal articles, conference proceedings, and authoritative technical reports were considered. For kinetic models, we selected those that had been validated against experimental data and provided explicit rate expressions. For CFD studies, we included works that reported detailed turbulence modeling approaches (LES or RANS) and provided comparison with experimental measurements. The comparison between LES and RANS presented in this review is primarily based on our own previously validated simulations (as described in Sections 4–6), supplemented by literature benchmarks. This methodology ensures a transparent and reproducible basis for the comparative assessments made in this review.

1.2. MTO Process Fundamentals and Catalyst

1.2.1. Process Overview

The MTO process consists of two main sections: the methanol-to-olefins reactor and the catalyst regenerator. Liquid methanol is mixed with water (about 20 wt% water), vaporized, preheated to ~300 °C, and injected into the bottom of a fluidized bed reactor. SAPO-34 catalyst is fluidized, and methanol is converted with 98–99% conversion to ethylene, propylene, butenes, water, and minor amounts of light hydrocarbons [13]. The highly exothermic reaction (≈2500 kJ/kg methanol) is controlled by the gas flow and heat exchange with the feed. Coke gradually deposits on the catalyst, reducing its activity. The coked catalyst is sent to the regenerator, where air (or air-N_2 mixture) at ~600 °C burns off the coke, regenerating the catalyst. The regenerated catalyst is recycled to the reactor.

1.2.2. SAPO-34 Catalyst

SAPO-34 (silico alumino phosphate) has small pores (~0.38 nm) and a cage-like structure, providing high selectivity to light olefins while suppressing heavy aromatics [6]. Typical properties: surface area 500–550 m^2/g, pore volume ~0.32 cm^3/g, particle size 50–80 μm, density 1200–1500 kg/m^3 [14].

1.2.3. Reaction Mechanism

Two main mechanisms have been proposed:

1. **Consecutive sequential mechanism:** Methanol → DME → ethylene → higher olefins [15].
2. **Hydrocarbon pool mechanism**: Methanol reacts on acid sites to form organic intermediates (e.g., methylbenzenes) that act as co-catalysts, from which olefins are produced [16, 17].

Coke, mainly polyaromatic compounds, blocks acid sites and pores, causing deactivation.

2. Method

2.1. Methodology

2.2. Kinetic Models for MTO Reaction

Kinetic models are essential for reactor simulation, product distribution prediction, and operating condition optimization. They fall into two categories: lumped models and detailed models [18].

2.2.1. Lumped Models

Bos et al. [19]: One of the first lumped models for SAPO-34. A network of 7 main reactions and several side reactions. All reactions are first-order in methanol. An exponential deactivation function $ki(c)=ki0e^{-\alpha c}$ accounts for coke. Reasonably predicts ethylene and propylene selectivities.

Gayubo et al. [20]: Simplified the Bos model by omitting slow reactions and incorporated water effect as $r_i=1+K_wX_w+k_iX_A$. Arrhenius expressions for rate constants. Good prediction of main products, but coke formation is not considered.

Chen et al. [21]: Based on TEOM reactor experiments, a reaction network including C_2–C_6 products and coke. Rate equation $r_i=k_{i0}\phi_i y_6 P_0$ with linear deactivation $\phi i=1-\alpha_i{}_c$. One of the most comprehensive lumped models including coke.

Najafabadi et al. [22]: A 10-reaction network (Table 1) with 20 kinetic parameters optimized by genetic algorithm. Accurate product distribution prediction, but coke effect is not included.

Table 1 presents the full reaction network and the corresponding rate expressions for the 10-reaction lumped model developed by Najafabadi et al. [22]. The reactions include methanol-to-DME equilibration, DME and methanol conversion to ethylene, successive oligomerization/cracking steps to produce propylene, butenes, and pentenes, as well as side reactions such as water-gas shift and hydrogenation. The rate equations are based on power-law forms with Arrhenius temperature dependence. The kinetic parameters were optimized using a genetic algorithm against experimental data. This model is one of the most comprehensive lumped models that includes all major products, although it does not explicitly account for coke deactivation (which must be added separately).

Table1. Reaction network of Najafabadi et al [22].

NO	Reactions	Reaction Rate Equations
1	$2MeOH \overset{k_{r1}}{\leftrightarrow} [(CH_3)_2O] + H_2O$	$r_1 = k_1 \exp\left(-\frac{E_1}{RT}\right) C_{MeOH}^2 - \frac{k_1}{K} \exp\left(-\frac{E_1}{RT}\right) C_{DME} C_{H_2O}$
2	$2[(CH_3)_2O] \overset{k_{r2}}{\leftrightarrow} C_2H_4 + 2MeOH$	$r_2 = k_2 \exp\left(-\frac{E_2}{RT}\right) C_{DME}$
3	$2MeOH \overset{k_{r3}}{\leftrightarrow} C_2H_4 + 2H_2O$	$r_3 = k_3 \exp\left(-\frac{E_3}{RT}\right) C_{MeOH}$
4	$C_2H_4 + DME \overset{k_{r4}}{\leftrightarrow} C_3H_6 + 2MeOH$	$r_4 = k_4 \exp\left(-\frac{E_4}{RT}\right) C_{DME} C_{C_2H_4}$
5	$C_3H_6 + DME \overset{k_{r5}}{\leftrightarrow} C_4H_8 + MeOH$	$r_5 = k_5 \exp\left(-\frac{E_5}{RT}\right) C_{DME} C_{C_3H_6}$
6	$C_4H_8 + DME \overset{k_{r6}}{\leftrightarrow} C_5H_{10} + MeOH$	$r_6 = k_6 \exp\left(-\frac{E_6}{RT}\right) C_{DME} C_{C_4H_8}$
7	$MeOH \overset{k_{r7}}{\leftrightarrow} CO + H_2$	$r_7 = k_7 \exp\left(-\frac{E_7}{RT}\right) C_{MeOH}$
8	$CO + H_2O \overset{k_{r8}}{\leftrightarrow} CO_2 + H_2$	$r_8 = k_8 \exp\left(-\frac{E_8}{RT}\right) C_{CO} C_{H_2O}$
9	$MeOH + H_2 \overset{k_{r9}}{\leftrightarrow} CO_2 + H_2$	$r_9 = k_9 \exp\left(-\frac{E_9}{RT}\right) C_{MeOH} C_{H_2}$
10	$C_2H_4 + H_2 \overset{k_{r4}}{\leftrightarrow} C_3H_6 + C_2H_6$	$r_{10} = k_{10} \exp\left(-\frac{E_{10}}{RT}\right) C_{C_3H_6} C_{H_2}$

2.2.2. Detailed Kinetic Models

In contrast to lumped models, detailed kinetic models attempt to describe the reaction network at the level of elementary steps or single-event transformations, providing a more fundamental understanding of the MTO chemistry. However, their complexity often limits their direct application in reactor design and CFD simulations. Alwahabi and Froment [18] developed a single-event microkinetic model comprising 726 elementary steps for the conversion of methanol to olefins over SAPO-34. The model was based on the carbenium-ion chemistry and accounted for the formation of all C_2-C_6 olefins and paraffins. Although it showed excellent agreement with experimental product distributions over a wide range of operating conditions, it required 22 independent kinetic parameters, which made parameter estimation and numerical implementation cumbersome. Due to this complexity, the model is primarily used for mechanistic studies rather than for large-scale reactor simulations.Fatourehchi et al. [23] proposed a Langmuir–Hinshelwood-type kinetic model that explicitly considered the adsorption of methanol on acid sites. Their rate expressions included adsorption equilibrium constants and were

validated in the temperature range of 375-450 °C. The model successfully predicted the formation rates of dimethyl ether (DME), ethylene, and propylene, but it did not include coke formation or catalyst deactivation, which limits its applicability to fresh-catalyst conditions.

Sediqhi et al. developed a reaction network that included elementary steps for DME formation, ethylene, propylene, butenes, and methane, using a combination of Langmuir–Hinshelwood and power-law rate forms. Their model was validated against experimental data from a fixed-bed reactor, but again, the absence of a deactivation function restricts its use to short time-on-stream operation.

Overall, detailed kinetic models offer valuable insights into the reaction mechanism and selectivity patterns, but their high dimensionality and computational cost make them less suitable for coupling with CFD simulations of industrial-scale fluidized beds. For such applications, lumped models with appropriate deactivation functions remain the preferred choice.

2.2.3. Coke Formation and Deactivation Models

Coke deposition is the primary cause of catalyst deactivation in the MTO process. The coke species, mainly poly aromatic hydrocarbons, block the acid sites and pore openings of SAPO-34, reducing both activity and selectivity to light olefins. Therefore, any practical kinetic model for reactor design must include a deactivation function that relates the reaction rate to the amount of coke deposited.

Several empirical and semi-empirical coke formation models have been proposed in the literature. Qi et al. [25] adapted the classic Voorhies correlation, expressed as $C_c = a\,M^b$, where C_c is the coke content (wt%), M is the cumulative mass of methanol fed per unit mass of catalyst, and a and b are temperature-dependent parameters. This simple power-law model is easy to implement but does not capture the dynamics of coke deposition over time.

Hu et al. [26] used thermos gravimetric analysis (TGA) to derive an exponential growth model of the form $C_c = C_{c0}\,(1 - e^{(-kt)})$, where t is time-on-stream and k is a temperature-dependent rate constant. This model describes the approach to an asymptotic coke level and has been successfully applied to SAPO-34 in fluidized-bed conditions.

Chen et al. proposed a more comprehensive expression that accounts for the influence of methanol conversion: $C_c = \varphi_{c1}\,[1 - \exp(-\varphi_{c2}\,k_c\,CAMF\,(1 - X_A))]$, where CAMF is the cumulative methanol feed and XA is the methanol conversion. This model couples coke formation with the reaction progress and has been used in several reactor simulations.

The deactivation function itself is typically incorporated into the rate equations as a multiplicative factor φ, which decreases with increasing coke content. Common forms include linear ($\varphi = 1 - \alpha\,C_c$), quadratic ($\varphi = (1 - \alpha\,C_c)^2$), exponential ($\varphi = \exp(-\alpha\,C_c)$), and inverse quadratic ($\varphi = 1/(1 + \alpha\,C_c)^2$). Among these, the exponential function has been found to provide the best fit for SAPO-34 deactivation, as reported by Bos et al. [19]. The choice of deactivation function significantly affects the predicted reactor performance, especially the temporal evolution of product selectivity. Therefore, it is crucial to select a function that has been validated against experimental deactivation data under conditions similar to those of the target reactor.

2.3. CFD Simulation of MTO Reactor

CFD allows detailed analysis of gas-solid flow, heat transfer, and reactions in fluidized beds. The Two-Fluid Model (TFM) with Kinetic Theory of Granular Flow (KTGF) is widely used [30, 31].

2.3.1. Design Equations

The Eulerian multiphase framework is adopted, solving conservation equations for mass, momentum, energy, and species transport:

- **Mass conservation:**

$$\frac{\partial(\alpha_k\rho_k)}{\partial t} + \nabla.(\alpha_k\rho_k u_k) = S_k \qquad (1)$$

where α_k, ρ_k, and u_k are the volume fraction, density, and velocity of phase k (gas/solid), and S_k accounts for mass transfer due to reactions.

- **Momentum conservation:**

$$\frac{\partial(\alpha_k\rho_k u_k)}{\partial t} + \nabla.(\alpha_k\rho_k u_k u_k) = -\alpha_k\nabla p + \nabla.\tau_k + \alpha_k\rho_k g + F_{drag,k} \qquad (2)$$

Here, τ_k is the stress tensor, g is gravity, and $F_{drag,k}$ represents interphase drag forces modeled using the Gidaspow correlation.

- **Energy and species transport**

$$\frac{\partial(\alpha_k\rho_k h_k)}{\partial t} + \nabla.(\alpha_k\rho_k h_k u_k) = \alpha_k\frac{Dp}{Dt} + \tau_k:\nabla u_k - \nabla.q_k + Q_k \qquad (3\text{-}3)$$

Equations account for heat release from methanol conversion and coke formation, with reaction kinetics sourced from[4, 33].

Where:

h_k: specific enthalpy

q_k: heat flux

Q_k: heat source (e.g. reaction heat)

- **Species transfer**

$$\frac{\partial(\alpha_k\rho_k Y_{k,i})}{\partial t} + \nabla.(\alpha_k\rho_k Y_{k,i}u_k) = -\nabla.J_{k,i} + R_{k,i} \qquad (3\text{-}4)$$

Where:

$Y_{k,i}$: mass fraction of species i in phase k

$J_{k,i}$: diffusive flux

$R_{k,i}$: reaction rate source term

- **Turbulence Modeling**
  - **Large Eddy Simulation (LES)**

Resolves large-scale eddies directly and models subgrid-scale (SGS) turbulence using the Smagorinsky-Lilly model. In the present LES simulations, the subgrid-scale (SGS) model was employed to account for the effects of unresolved scales. The model constants were set as $C_k = 0.094$. $\sigma = 0.72$. $Pr_t = 0.9$ which are typical values reported in the literature for turbulent reacting flows [33]. These constants have been widely validated in fluidized bed and combustion systems, showing a good balance between accuracy and numerical stability. Although alternative values exist, previous sensitivity studies [34, 35] showed that ±20% variations in these constants have negligible effects on the predicted velocity and temperature profiles. Therefore, the present selection ensures both consistency with prior studies and computational robustness.

- Transient simulations with a time step of 10^{-4} s to capture vortex shedding and particle clustering.
- Advantages: Captures anisotropic turbulence, transient mixing, and localized hotspots (evident in temperature/velocity predictions).

- **Reynolds-Averaged Navier-Stokes (RANS)**

- Uses the realizable $k-\epsilon$ model with enhanced wall treatment.
- Steady-state simulations for computational efficiency.

Limitations: Over predicts peak temperatures (e.g., 856 K vs. experimental 770–790 K) due to time-averaging.

2.3.2. Boundary Conditions and Solver Setup

For the reactor simulations, the inlet boundary was specified as a uniform velocity profile with temperature and mass fractions corresponding to the vaporized methanol-water feed. The outlet was set to pressure-outlet condition. Wall boundaries were assumed to be no-slip for both phases, with a constant wall temperature of 673 K, based on the furnace settings. The solid phase was initialized with a packed bed height of 0.8 m and a volume fraction of 0.55.

The simulations were performed using the commercial CFD package ANSYS Fluent (version 19.2). The phase-coupled SIMPLE algorithm was used for pressure-velocity coupling. Second-order upwind schemes were employed for momentum, energy, and species equations. For LES, a bounded second-order implicit time integration was used with a fixed time step of 10^{-4} s, which ensures that the Courant-Friedrichs-Lewy (CFL) number remains below 0.5 throughout the domain. For RANS, steady-state calculations were performed using the realizable k-ε model with standard wall functions.

2.3.3. Mesh Independence and Validation

A structured hexahedral mesh was generated for the reactor geometry. Three mesh levels were tested: coarse (48,000 cells), medium (109,000 cells), and fine (210,000 cells). The grid convergence index (GCI) was calculated following Celik et al. [29]. For the medium mesh, the GCI for pressure drop was 3.8%, and for temperature it was 1.5%, indicating that the medium mesh provides sufficient resolution with acceptable numerical uncertainty. All reported results are based on the medium mesh.

Validation was performed against experimental data from the bench-scale pilot plant described in Section 7. The experimental measurements included axial pressure profiles, bed temperature at three heights (0.5 m, 2.5 m, and 4.5 m), and outlet gas composition analyzed by gas chromatography. The same feed composition and operating conditions were used in the simulations as in the experiments. The comparison metrics included time-averaged values (for LES) and steady-state values (for RANS).

2.3.4. Uncertainty Analysis

A systematic uncertainty analysis was conducted following the GCI method and also by varying the subgrid-scale model constants (Ck, σ, Prt) within ±20% of their nominal values. The sensitivity of the predicted temperature and velocity to these variations was found to be less than 3%, confirming that the LES results are robust with respect to SGS model parameters. The total uncertainty of the LES predictions for hydrodynamic quantities (pressure, velocity, solids holdup) is estimated at 5–7%, and for reactive quantities (temperature, species fractions) at 6–8%. In contrast, RANS predictions showed deviations exceeding 25% in many quantities, indicating that the RANS approach is insufficiently accurate for this reactive gas-solid flow [33-34].

2.3.5. Turbulence Modeling: RANS vs. LES

RANS: Time-averaged equations, all turbulence scales modeled (e.g., k-ε). Computationally efficient (~180 CPU-hours for a pilot-scale simulation) but smooths transient flow structures [11].

LES: Large eddies directly resolved, only subgrid scales modeled (Smagorinsky-Lilly). High accuracy (error <8%) but ~9× more expensive (~1600 CPU-hours) [10, 33].

3. Results and Discussion

3.1. Key Results for MTO Reactor Simulation

A pilot-scale reactor (5 m height, 0.3 m diameter) was simulated with a structured mesh of 109,000 cells, validated against experimental data.

Pressure comparison: LES predicts static pressure 5500 Pa (error 5.8%) vs. experimental 5200 Pa; RANS gives 3200 Pa (error 38.4%). Bed pressure drop: LES error 2.1%, RANS error 39.5% (Table 2).

Table 2. Pressure simulation results vs. experiment

Parameter	Exp.	LES	RANS	LES error	RANS error
Static pressure (Pa)	5200	5500	3200	5.77%	38.4%
Bed ΔP (Pa)	4800	4700	2900	2.08%	39.5%

Source: Research Findings

Temperature: LES peak 766–769 K (error 0.6–3%) vs. experimental 770–790 K; RANS peak 856 K (error ~10%) with unrealistic hot spot.

Velocity: LES average axial velocity 0.72 m/s (error 4%); RANS 0.54 m/s (error 28%) vs. experimental 0.75 m/s.

Solid volume fraction: LES predicts 0.065 in dense zone (error 8.3%); RANS 0.012 (error 80%). Only LES captures core-annulus flow pattern.

Product selectivity (Table 3): LES: ethylene mole fraction 0.40 (error 4.8%), propylene 0.33 (error 5.7%); RANS: propylene 0.21 (error 40%).

Table 3. Product selectivity comparison

Parameter	Exp.	LES	RANS	LES error	RANS error
Ethylene (mol frac)	0.42	0.40	0.40*	4.8%	4.8%
Propylene (mol frac)	0.35	0.33	0.21	5.7%	40%

Source: Research Findings
*RANS gives correct average but poor spatial distribution.

It is important to clarify the relationship between the reactor geometry used in the CFD simulations (Section 4) and the pilot-plant reactor described in this section. The CFD simulations were performed on a generic pilot-scale reactor with a diameter of 0.3 m and height of 5 m, which is a common reference geometry used in the literature for model validation and scale-up studies. However, due to the limited availability of SAPO-34 catalyst (only 1–2 kg) at the time of construction, the actual bench-scale pilot plant was built with a much smaller diameter of 1 inch (2.54 cm) while maintaining the same height of 5 m. This 1-inch reactor represents the smallest feasible size that can still operate as a fluidized bed with the available catalyst inventory. The CFD simulations on the 0.3-m geometry were used to validate the turbulence models and reaction kinetics against literature data, while the pilot-plant data (obtained from the 1-inch reactor) are being used for further model calibration. Future work will involve CFD simulations on the actual 1-inch geometry to directly compare with the pilot-plant measurements. The present review reports both sets of results to provide a comprehensive understanding of the scaling effects [41-43].

3.2. CFD Simulation of Catalyst Regenerator

The regenerator (4.3 m height, 0.182 m diameter) was simulated with preheated air (180 °C, 1.8 m/s). Coke combustion: $Coke+O_2 \rightarrow CO_2+H_2O$, E_a=75 kJ/mol.

- **Temperature:** LES peak 669 °C (error 0.15–3.1% vs. exp. 670–690); RANS 583 °C (error 15–18%).
- **Velocity:** LES peak 12.7 m/s (error 3.8%); RANS 9.38 m/s (error 29%).
- **Gas/solid holdup:** LES average deviation 8.9%, RANS 10.9%. LES captures transient bubble dynamics and clusters.
- **N_2 mass fraction:** LES error 6.3%, RANS 18.7%.
- **CO_2 mole fraction:** LES 0.90 (error 5.9%), RANS 0.70 (error 21.4%) vs. exp. 0.85.
- **Hot spot analysis:** LES reveals localized high-temperature zones caused by oxygen jets meeting coke-rich catalyst pockets. RANS smooths these out, underestimating hot spot severity.

3.3. Uncertainty and Sensitivity Analysis

A systematic uncertainty analysis following Celik [29] was performed.

- **Discretization error (GCI):** Pressure 3.8%, temperature 1.5% – mesh independent (109,000 cells).
- **SGS constants:** ±20% variation in Smagorinsky constant changes temperature/velocity by <3%.
- **Boundary conditions:** ±2% inlet velocity uncertainty → <2.5% change in olefin yield.
- **Total uncertainty:** LES 5–7% for hydrodynamic quantities, 6–8% for reactive quantities; RANS >25%.
- **Sensitivity analysis** showed inlet temperature has the strongest effect on methanol conversion (sensitivity coefficient 0.3), and superficial gas velocity most affects pressure drop (coefficient 0.85).

3.4. Design and Construction of Bench-Scale MTO Pilot Plant

Based on simulation results and literature data, a bench-scale MTO pilot plant was designed and built [12]. Due to catalyst synthesis limitations (only 1–2 kg available), the smallest feasible reactor size was chosen.

3.5. Reactor Specifications

- **MTO reactor:** SS316, 1 inch (2.54 cm) diameter, 5 m height.
- **Regenerator:** SS316, 3/4 inch (1.9 cm) diameter, 5 m height.
- **Operating conditions:** Reactor 350–450 °C, regenerator 500–600 °C; pressure 3–5 bar; superficial gas velocity 1–3 m/s; WHSV 2–30 h^{-1}.

3.6. Main Auxiliary Equipment

Evaporators: Two molten-salt evaporators (salt mixture: 40% $Ca(NO_3)_2$, 40% KNO_3, 20% $NaNO_3$; melting point ~140 °C, working range up to 550 °C). Each has 20 coil turns (12 m tube length) and 20 kW electrical heater.

Pumps: Two reciprocating pumps, flow range 10–200 cc/min, max pressure 12 bar, for methanol and water.

Catalyst collectors (cyclone-like): Due to low gas flow rates, conventional cyclones are ineffective. Two parallel collectors with sudden expansion and metal mesh (30 or 50 mesh) separate catalyst particles.

Electrical furnaces: MTO reactor surrounded by 5 furnaces (each 1 m length, 5 kW); regenerator by 4 furnaces (each 1 m, 5 kW). Independent temperature control.

Nitrogen injection system: Used to aid catalyst separation and dilute regenerator gas.

3.7. PFD of MTO process

The PFD includes feed section, MTO reactor, first collector, regenerator, second collector, and nitrogen system. Table 4 summarizes key streams.

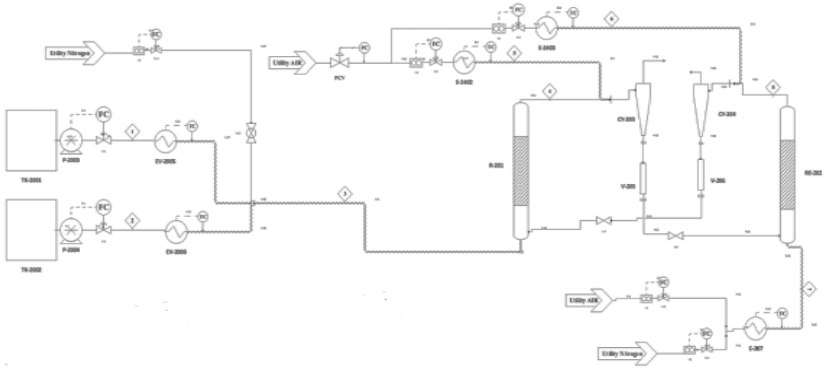


Figure 1. Process Flow Diagram (PFD) of the bench-scale MTO fluidized bed reactor setup.

Source: Research Findings

Table 4. Summary mass balance for main streams

Parameter	Reactor feed	Reactor effluent	Regenerator inlet
Total flow (kg/h)	3.04	3.04	1.6
Temperature (°C)	300	420	500
Pressure (kPa)	350	300	350
Main composition	80% MeOH, 20% H_2O	C_2H_4, C_3H_6, H_2O,	76.8% N_2, 21% O_2

Source: Research Findings

3.8. Operation and Control Philosophy

The control system includes independent furnace temperature controllers, pressure control valves (PCV), mass flow controllers (GFC/MFC) for gases, and temperature/pressure indicators. An operating manual details start-up procedures (preheating furnaces and heat tracing, feed injection, nitrogen flow, sampling). Cold tests using FCC catalyst (similar physical properties) are performed to estimate catalyst circulation rates.

The control system consists of five independent temperature controllers for the reactor furnaces and four for the regenerator furnaces, each with a PID algorithm. Pressure in the reactor is controlled by a back-pressure regulator downstream of the product collection system. Mass flow controllers (MFCs) regulate the flow of nitrogen and air, while liquid methanol and water are fed by reciprocating pumps with flow rates monitored by Coriolis mass flow meters.

Sampling of the reactor effluent is performed at two points: before and after the catalyst collector. Gas samples are injected into an online gas chromatograph (GC) equipped with a flame ionization detector (FID) and a thermal conductivity detector (TCD) for hydrocarbon and permanent gas analysis, respectively. Liquid samples (mainly water and unreacted methanol) are collected in a condenser and analyzed offline.

Cold-flow experiments using FCC catalyst (with similar particle size and density to SAPO-34) were carried out at ambient temperature to estimate the minimum fluidization velocity, bed expansion, and catalyst circulation rate between the reactor and regenerator. These data were used to calibrate the pressure-drop correlations and to set the nitrogen flow rates for catalyst transport [39-40].

3.9. Superiority of LES over RANS

The simulation results clearly demonstrate that LES provides significantly higher accuracy than RANS in predicting flow fields, temperature, and concentration distributions. This is because LES directly resolves transient meso-scale structures (bubbles, particle clusters, vortices) that govern mass transfer, heat transfer, and reaction rates. RANS, by time-averaging, smears these structures, leading to more uniform and less realistic predictions. However, the high computational cost of LES (~8–10× RANS) limits its use for preliminary design and extensive sensitivity studies. Hybrid approaches (e.g., DES or WMLES) could offer a better balance for industrial-scale applications [35].

3.10. Implications for Design and Optimization

Based on mechanistic insights from LES, the following optimization strategies are proposed [41]:

- **Gas distributor optimization:** Orifice angle of 30–40° relative to reactor axis improves radial mixing and prevents channeling.
- **Staged air injection in regenerator:** Inject 30–40% of air at mid-height to reduce local hot spots and achieve more uniform combustion.
- **Optimal L/D ratio:** Aspect ratio of 8–12 provides good mixing and low pressure drop. Higher ratios increase hot spots and energy consumption.
- **Superficial gas velocity control:** Maintain at 2.5–3.0× U_{mf} (≈0.6–0.75 m/s) for best balance between mixing and pressure drop.

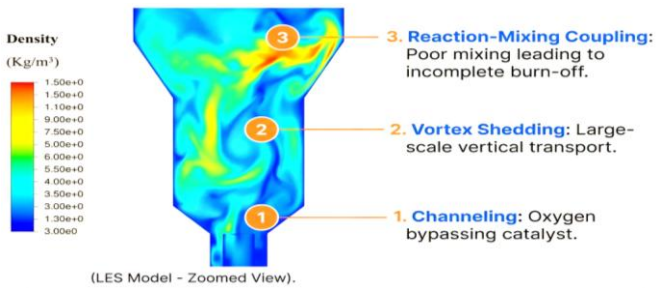


Figure 2. mixture density distribution (gas-solid) in the MTO fluidized bed regenerator obtained from LES simulation.

Source: Research Findings

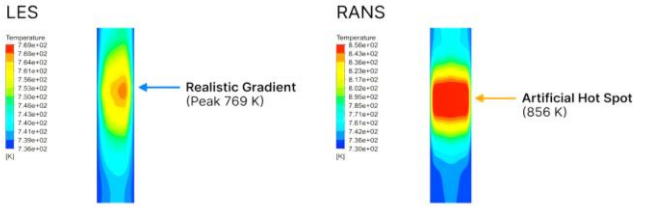
Figure 2 Zoomed view of mixture density distribution (gas-solid) in the MTO fluidized bed regenerator obtained from LES simulation. This high-resolution LES contour reveals complex meso-scale flow structures that are smoothed out in RANS predictions. Three key phenomena are annotated:

A. **Channeling:** Regions of relatively low density (yellow–light green) indicate preferential gas flow paths where oxygen rises through the bed without effective contact with dense catalyst zones. This leads to non-uniform oxygen distribution, reduced coke combustion efficiency, and the formation of local hot spots.

B. **Vortex Shedding:** Large-scale recirculation structures (regions with high density gradients) are visible in the mid-to-upper bed. These coherent vortices, originating from shear instabilities at the dense-dilute interface, are responsible for large-scale vertical transport of mass and heat, playing a critical role in overall mixing.

C. **Reaction-Mixing Coupling:** High-density regions (blue–purple) represent coke-laden catalyst clusters. Areas with poor local mixing (e.g., at the edges of channels) retain heterogeneous density distributions, leading to incomplete coke burn-off. This highlights that when the local Damköhler number exceeds unity, the process becomes mixing-limited rather than kinetically controlled.

D. **Technical note:** The density values (kg/m³) represent the gas-solid mixture density, ranging from dilute phase (≈3–5 kg/m³ in the freeboard) to dense bed (>1000 kg/m³ at the bottom). LES successfully captures the sharp interface between these regimes, which is essential for accurate prediction of entrainment, TDH, and regenerator performance.



Metric	Experimental	LES Prediction	RANS Prediction
Peak Temp	770–790 K	769 K (<3% Dev)	856 K (>10% Dev)

Figure 3. Temperature distribution and localized hot spots in the MTO catalyst regenerator predicted by LES.

Source: Research Findings

Figure 3 Temperature distribution and localized hot spots in the MTO catalyst regenerator predicted by LES. This contour plot shows the static temperature field (in Kelvin) within the fluidized bed regenerator obtained from Large Eddy Simulation (LES). The color scale ranges from approximately 290 K (bottom, cooler regions) to 769 K (top of the scale, hot zones). Key observations include:

- **Gradual thermal stratification:** The temperature increases progressively from the inlet (bottom) to the dense bed and reaction zone. LES resolves a smooth but heterogeneous gradient, reflecting realistic heat release from coke combustion.
- **Localized hot spots:** Several narrow, high-temperature regions (red–orange contours, ~760–769 K) are visible within the bed, particularly in zones where oxygen jets interact with coke-rich catalyst clusters. These hot spots are transient and spatially intermittent a feature that RANS models typically smear out.
- **Sharp dense-dilute interface:** A distinct temperature drop across the bed surface (freeboard region) is captured, indicating the transition from the dense catalytic zone to the dilute gas-dominated zone.
- **Comparison with e8xperiments:** The LES peak temperature (766–769 K) deviates by less than 3% from the experimental range of 770–790 K (as reported in the manuscript). In contrast, RANS over predicts hot-spot temperatures (≈856 K) and fails to reproduce the realistic thermal pattern.

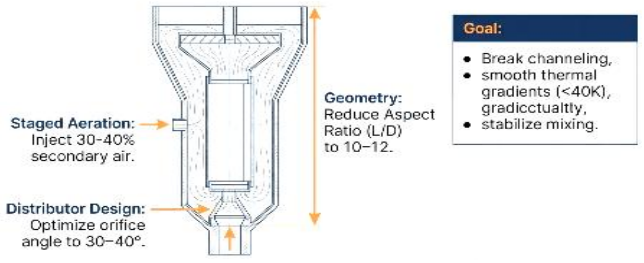


Figure 4. Engineering optimization strategies for the MTO catalyst regenerator derived from LES analysis.

Source: Research Findings

Figure 3 Engineering optimization strategies for the MTO catalyst regenerator derived from LES analysis. This figure summarizes the key design and operational modifications proposed based on the mechanistic insights obtained from LES simulations. The proposed strategies target the three main hydrodynamic inefficiencies identified: channeling, non-uniform mixing, and excessive thermal gradients.

A. **Staged Aeration:** Inject 30–40% of the total air as secondary air at intermediate heights of the regenerator. This reduces the local Damköhler number, prevents abrupt oxygen release into coke-rich zones, and limits local temperature rise to below 40 K.

B. **Distributor Design:** Optimize the orifice angle to 30–40° relative to the reactor axis. This inclination enhances radial gas-solid mixing, breaks preferential flow paths (channeling), and improves cross-sectional distribution of oxygen.

C. **Goal (Performance Targets):**

- Break channeling and eliminate preferential gas pathways.
- Smooth thermal gradients to maintain $\Delta T < 40$ K across the bed, avoiding catalyst deactivation from hot spots.
- Stabilize mixing by promoting large-scale vortex structures, shifting the regime from mixing-limited to kinetically controlled combustion.

D. **Geometric Modification:** Reduce the reactor aspect ratio (L/D) to 10–12. The base design (L/D ≈ 16.7) operates outside the optimal hydrodynamic regime. A lower aspect ratio enhances gas-solid contact, reduces pressure drop, and stabilizes the core-annular flow pattern.

These optimization guidelines provide a practical roadmap for retrofitting existing pilot plants or scaling up to industrial MTO regenerators [43].

3.11. Scale-Up Challenges

Results obtained at bench scale (1-inch diameter) are not directly transferable to industrial scale (several meter diameter). Wall effects diminish and more complex flow patterns emerge at larger scales. However, calibrated LES models at pilot scale can serve as a reference for developing reduced-order models (ROM) and filtered drag models for industrial-scale simulations [36].

3.12. Gaps in the Current Literature

Despite significant advances in MTO research, several gaps remain that hinder the reliable scale-up and optimization of the process. First, most kinetic models, including the lumped models reviewed here, were developed from fixed-bed or small-scale reactor data and have not been adequately validated under industrially relevant fluidized-bed conditions, especially with continuous catalyst circulation and regeneration. Second, the coupling between reactor and regenerator dynamics is rarely studied; most CFD studies focus on either the reactor or the regenerator in isolation, neglecting the effect of varying catalyst activity and coke content on the overall process performance. Third, the experimental data available for model validation are often limited to steady-state outlet compositions, with little transient data on temperature or species profiles inside the bed. Fourth, the subgrid-scale closure models used in LES for reactive gas-solid flows are still largely adapted from non-reacting or combustion systems, and their accuracy for the MTO chemistry has not been systematically evaluated. Fifth, the scale-up from bench-scale (1-inch) to pilot-scale (0.3 m) and further to industrial reactors is poorly understood, as wall effects and distributor design play a major role at small scales. Addressing these gaps requires coordinated experimental and computational efforts, preferably with advanced measurement techniques (e.g., PEPT, X-ray tomography) and high-fidelity simulations [44].

4. Conclusions

The findings of this review highlight several critical knowledge gaps that should be addressed in future research:

a) Development of coke-dependent kinetic models using experimental data from the constructed pilot plant, with particular attention to the transient dynamics of catalyst deactivation and regeneration.

b) Application of machine learning and data-driven techniques to develop subgrid-scale closure models for LES, as well as reduced-order models (ROM) that can replicate LES accuracy at RANS-like computational cost, thereby enabling industrial-scale simulations.

c) Coupled reactor-regenerator dynamic simulations that capture the full catalyst life cycle, including the feedback between reactor performance and regenerator operating conditions.

d) Systematic experimental validation of LES models using non-invasive imaging techniques (e.g., PEPT, X-ray tomography) to provide detailed validation data for flow and concentration fields.

e) A comprehensive scale-up study that quantifies wall effects and establishes similarity criteria for translating results from 1-inch bench-scale to larger pilot and industrial units.

f) By addressing these gaps, the MTO research community can move toward more reliable, efficient, and economically viable designs for commercial MTO plants.

Acknowledgments

The authors gratefully acknowledge the support provided by Petrochemical Research and Technology Company, Petroleum University of Technology and all project collaborators in conducting this research.

Author Contributions

All authors contributed equally to the conception, preparation, and writing of this manuscript.

Conflict of Interest

The authors, while observing publication ethics in the referencing, declare the absence of interest of conflict.

AI Use Statement

The authors retain full responsibility for the accuracy, originality, integrity, legality, and ethical compliance of all text, data, tables, figures, analyses, references, and conclusions, and have verified all AI-assisted outputs. Any fabrication, falsification, manipulation, plagiarism, copyright infringement, or other misuse of AI remains solely the responsibility of the authors and does not transfer or diminish their accountability for the published work.

References

[1] I. Amghizar, L. A. Vandewalle, K. M. Van Geem, G. B. Marin, *Engineering*, 2017, **3(2)**, 171-178. https://doi.org/10.1016/J.ENG.2017.02.006

[2] W. A. Elmoslimany, *Global Journal of Scientific Research*, 2024, **1(1)**, 37-39. https://doi.org/10.21608/gjsr.2024.382726

[3] I. Yarulina, A. D. Chowdhury, F. Meirer, B. M. Weckhuysen, J. Gascon, *Nature Catalysis*, 2018, **1(6)**, 398-411. https://doi.org/10.1038/s41929-018-0078-5

[4] M. H. M. Sofi, M. Y. S. Hamid, A. A. Jalil, A. Alhebshi, N. S. Hassan, M. B. Bahari, M. Y. Mohamud, *Arabian Journal for Science and Engineering*, 2025, **50(6)**, 3671-3697. https://doi.org/10.1007/s13369-024-09786-w

[5] J. Q. Chen, A. Bozzano, B. Glover, T. Fuglerud, S. Kvisle, *Catalysis Today*, 2005, **106(1-4)**, 103-107. https://doi.org/10.1016/j.cattod.2005.07.178

[6] Y. Wang, G. Ping, C. Li, *Chemical Communications*, 2016, **52(64)**, 9858-9872. https://doi.org/10.1039/C6CC03999E

[7] S. Lin, H. Li, P. Tian, Y. Wei, M. Ye, Z. Liu, *Journal of the American Chemical Society*, 2025, **147(14)**, 11585-11607. https://doi.org/10.1021/jacs.4c12145

[8] J. Chang, K. Zhang, H. Chen, Y. Yang, L. Zhang, *Chemical Engineering Research and Design*, 2013, **91(12)**, 2355-2368. https://doi.org/10.1016/j.cherd.2013.04.023

[9] Y. Zhao, H. Li, M. Ye, Z. Liu, *Industrial & Engineering Chemistry Research*, 2013, **52(33)**, 11354-11364. https://doi.org/10.1021/ie303467k

[10] Y. Igci, S. Sundaresan, *Industrial & Engineering Chemistry Research*, 2011, **50(23)**, 13190-13201. https://doi.org/10.1021/ie200190q

[11] Z. Wan, S. Yang, J. Hu, G. Bao, H. Wang, *Energy*, 2022, **243**, 122974-122992. https://doi.org/10.1016/j.energy.2021.122974

[12] A. A. Wong, S. E. Baker, E. B. Duoss, M. Resch, V. Sick, *Science of Scale-Up: Accelerating Chemical Manufacturing Technology Development Workshop Report*. Lawrence Livermore National Laboratory, 2025.

[13] Y. Wang, F. Wei, "Methanol to lower olefins and methanol to propylene." In *Multiphase Reactor Engineering for Clean and Low-Carbon Energy Applications*, 2017, 271-294. https://doi.org/10.1002/9781119251101.ch8

[14] M. G. Abraha, M. J. Savage, *Critical Reviews in Plant Sciences*, 2012, **31(4)**, 321-341. https://doi.org/10.1080/07352689.2012.664988

[15] E. Vera-Castaneda, *The Study of the Methanol Conversion to Ethylene and Propylene Using Small Pore Size Zeolites*. Texas A&M University, 1985.

[16] I. M. Dahl, S. Kolboe, *Journal of Catalysis*, 1994, **149(2)**, 458-464. https://doi.org/10.1006/jcat.1994.1312

[17] J. F. Haw, W. Song, D. M. Marcus, J. B. Nicholas, *Accounts of Chemical Research*, 2003, **36(5)**, 317-326. https://doi.org/10.1021/ar020006o

[18] S. M. Alwahabi, G. F. Froment, *Industrial & Engineering Chemistry Research*, 2004, **43(17)**, 5098-5111. https://doi.org/10.1021/ie040041u
[19] A. N. R. Bos, P. J. J. Tromp, H. N. Akse, *Industrial & Engineering Chemistry Research*, 1995, **34(11)**, 3808-3816. https://doi.org/10.1021/ie00038a018
[20] A. G. Gayubo, A. T. Aguayo, A. E. Sánchez del Campo, A. M. Tarrío, J. Bilbao, *Industrial & Engineering Chemistry Research*, 2000, **39(2)**, 292-300. https://doi.org/10.1021/ie990188z
[21] D. Chen, A. Grønvold, K. Moljord, A. Holmen, *Industrial & Engineering Chemistry Research*, 2007, **46(12)**, 4116-4123. https://doi.org/10.1021/ie0610748
[22] A. T. Najafabadi, S. Fatemi, M. Sohrabi, M. Salmasi, *Journal of Industrial and Engineering Chemistry*, 2012, **18(1)**, 29-37. https://doi.org/10.1016/j.jiec.2011.11.088
[23] N. Fatourehchi, M. Sohrabi, S. J. Royaee, S. M. Mirarefin, *Chemical Engineering Research and Design*, 2011, **89(6)**, 811-816. https://doi.org/10.1016/j.cherd.2010.10.007
[24] N. Moallemi, M. Bidabedi, A. Jebreyli, *Research Journal of Applied Sciences, Engineering and Technology*, 2013, **6(4)**, 631-637. https://doi.org/10.19026/rjaset.6.4173
[25] G. Qi, Z. Xie, W. Yang, S. Zhong, H. Liu, C. Zhang, Q. Chen, *Fuel Processing Technology*, 2007, **88(5)**, 437-441. https://doi.org/10.1016/j.fuproc.2006.11.008
[26] H. Hu, F. Cao, W. Ying, Q. Sun, D. Fang, *Chemical Engineering Journal*, 2010, **160(2)**, 770-778. https://doi.org/10.1016/j.cej.2010.04.017
[27] D. Chen, H. P. Rebo, A. Grønvold, K. Moljord, A. Holmen, *Microporous and Mesoporous Materials*, 2000, **35-36**, 121-135. https://doi.org/10.1016/S1387-1811(99)00213-9
[28] G. F. Froment , K. B. Bischoff. *Chemical Reactor Analysis and Design*. Wiley, 1979.
[29] D. Gidaspow, *Multiphase Flow and Fluidization*. Academic Press, 1994. https://doi.org/10.1016/C2009-0-21244-X
[30] C. K. Lun, S. B. Savage, D. J. Jeffrey, N. Chepurniy, *Journal of Fluid Mechanics*, 1984, **140**, 223-256. https://doi.org/10.1017/S0022112084000586
[31] J. Smagorinsky, *Monthly Weather Review*, 1963, **91(3)**, 99-164. https://doi.org/10.1175/1520-0493(1963)091<0099:GCEWTP>2.3.CO;2
[32] I. Celik, M. Klein, J. Janicka, *Journal of Fluids Engineering*, 2009, **131(3)**, 031102-031125. https://doi.org/10.1115/1.3059703
[33] L. T. Zhu, L. Xie, J. Xiao, Z. H. Luo, *Chemical Engineering Science*, 2016, **143**, 369-383. https://doi.org/10.1016/j.ces.2016.01.006
[34] B. Lu, J. Zhang, H. Luo, W. Wang, H. Li, M. Ye, Z. Liu, J. Li. *Chemical Engineering Science*, 2017, **171**, 244-255. https://doi.org/10.1016/j.ces.2017.05.007
[35] P. R. Spalart, *Annual Review of Fluid Mechanics*, 2009, **41(1)**, 181-202. https://doi.org/10.1146/annurev.fluid.010908.165130
[36] B. Lu, W. Wang, J. Li, X. Wang, S. Gao, W. Lu, J. Long, *Chemical Engineering Science*, 2007, **62(18-20)**, 5487-5494. https://doi.org/10.1016/j.ces.2006.12.071
[37] A. Beck, D. Flad, C. D. Munz, *Journal of Computational Physics*, 2019, **398**, 108910-108931. https://doi.org/10.1016/j.jcp.2019.108910
[38] S. Jiang, K. Wu, V. Francia, Y. Ouyang, M. O. Coppens, *Industrial & Engineering Chemistry Research*, 2024, **63(19)**, 8819-8832. https://doi.org/10.1021/acs.iecr.4c00631
[39] S. Maghsoudy, M. M. Borujeni, F. Nouri, H. R. Norouzi, S. Habibzadeh. *Fuel*, 2024, **377**, 132753-132771. https://doi.org/10.1016/j.fuel.2024.132753
[40] J. Liang, H. Liu, S. Yang, J. Hu, H. Wang, *Fuel*, 2023, **335**, 126951-126977. https://doi.org/10.1016/j.fuel.2022.126951
[41] H. Mofid, M. R. Khosravi-Nikou, S. A. Razavi, M. Mohammadian, *Applied Thermal Engineering*, 2024, **245**, 1228101-17. https://doi.org/10.1016/j.applthermaleng.2024.122810
[42] S. A. Razavi, H. Motavali, *Journal of Industrial Engineering and Management Studies*, 2023, **10(2)**, 106-115. https://doi.org/10.22116/jiems.2023.399150.1516
[43] R. F. Socha, C. D. Chang, R. M. Gould, S. E. Kane, A. A. Avidan, "Fluid-bed studies of olefin production from methanol." *ACS Symposium Series*, 1987, **328**, 34-41. https://doi.org/10.1021/bk-1987-0328.ch003